The intruder feature of ^{31}Mg and the coexistence of many particle and many hole states

M. Kimura
Institute of Physics, University of Tsukuba, Tsukuba 305-8571, Japan¡
(Dated: February 9, 2008)

The low-lying level structure of ^{31}Mg has been investigated by the antisymmetrized molecular dynamics (AMD) plus generator coordinate method (GCM) with the Gogny D1S force. It is shown that the N=20 magic number is broken and the ground state has the pure neutron $2p3h$ configuration. The coexistence of many particle and many hole states at very low excitation energy is discussed.

PACS numbers: Valid PACS appear here

The breakdown of the neutron magic number N=20 and the change of the shell order in neutron rich nuclei have been one of the great interest in nuclear structure studies. Experimentally, it was firstly pointed out from the observation of the anomalous binding energy and spin-parity of ^{31}Na [1, 2]. More convincing evidence was given by the observation of the small excitation energy [3, 4] and the large $E2$ transition probability [5] of the 2^+_1 state of ^{32}Mg. Theoretically, the Hartree-Fock calculation [6] showed that shape transition from spherical to prolate shapes possibly took place in neutron-rich N=20 nuclei. Shell model calculations [7, 8, 9] that allowed particle hole excitations across the N=20 shell gap explained these abnormal properties and suggested strong deformation of ^{31}Na and neighboring nuclei caused by the inversion between the normal and intruder configurations. Since then, many experimental [10, 11, 12, 13, 14, 15, 16, 17] and theoretical [18, 19, 20, 21, 22, 23, 24, 25, 26, 27, 28] studies have been made and now the systematic breaking of N=20 magic number is theoretically investigated and some of them are observed. Thus, our knowledge of the breakdown of the neutron magic number N=20 in the neutron rich nuclei has been increasing rapidly in this decade.

To understand the shell structure and the shell order, the odd-neutron nuclei such as ^{31}Mg and ^{29}Ne will provide essential information, since the property of the single particle orbital of the last neutron particle or hole will be strongly reflected to the property of total system. Recently the spin-parity of the ground state of ^{31}Mg was experimentally fixed to $1/2^+$ [16]. This result suggests that the ground state of ^{31}Mg has the intruder configuration in which two neutron occupy the pf-orbital and a neutron hole is in the Nilsson orbital [200,1/2]. However, mainly because of the limitation of the models, theoretical investigation of odd-neutron nuclei is not as vigorous as that of even-even nuclei. Indeed, there are only a few shell model calculations [16, 17, 18, 19] for ^{31}Mg, and they do not reproduce the ground state properties or they study the ground band and a few excited states using the modified interaction to reproduce the ground state properties.

In this work, we discuss the structure of the ^{31}Mg based on the theoretical framework of AMD+GCM [29, 32]. Since we do not assume the time reversal symmetry and we perform the parity projection before the variation, we can appropriately investigate the positive- and negative-parity states and the coexistence of the many particle-hole states in odd-mass nuclei. It will be shown that the ground state of ^{31}Mg has the pure intruder configuration that has the $2p3h$ configuration with respect to the N=20 shell closure. We have successfully reproduced the observed properties of ^{31}Mg such as the magnetic moment and the β-decay strengths. We also predict that other many particle-hole states ($0p1h$, $1p2h$ and $3p4h$) also coexist at very small excitation energy.

In the AMD, the intrinsic wave function is given by a Slater determinant of the single particle wave packets,

$$\Phi_{\rm int} = \mathcal{A}\{\varphi_1, \varphi_2, ..., \varphi_A\}, \quad \varphi_i(\mathbf{r}) = \phi_i(\mathbf{r})\chi_i\xi_i,$$

where φ_i is the ith single particle wave packet consisting of the spatial ϕ_i, spin χ_i and isospin ξ_i parts. The local Gaussian located at $\mathbf{Z}_i$ is employed as ϕ_i.

$$\begin{aligned}\phi_i(\mathbf{r}) &= \exp\Big\{-\sum_{\sigma=x,y,z}\nu_\sigma\Big(r_\sigma - \frac{\mathrm{Z}_{i\sigma}}{\sqrt{\nu_\sigma}}\Big)^2\Big\},\\ \chi_i &= \alpha_i\chi_\uparrow + \beta_i\chi_\downarrow, \quad |\alpha_i|^2 + |\beta_i|^2 = 1,\\ \xi_i &= \text{proton} \quad \text{or} \quad \text{neutron}.\end{aligned}$$

Here the centroids of the Gaussian $\mathbf{Z}_i$, the spin direction α_i and β_i and the width parameters ν_x, ν_y and ν_z are the variational parameters. As the variational wave function, we employ the parity projected wave function, $\Phi^\pi = \hat{P}^\pi\Phi_{\rm int}$. The Gogny D1S force [33] is employed as an effective nuclear force $\hat{V}_n$. Coulomb force $\hat{V}_c$ is approximated by the sum of seven Gaussians.

The calculation is performed in the following three steps. First, we carry out the energy variation and optimize the variational parameters. The energy variation is made under the constraint on the matter quadrupole deformation β to obtain the optimum wave function $\Phi^\pi(\beta)$ for given value β. We note that in this calculation, we do not make any assumption on the spatial symmetry of the wave function and do not put any constraint on the quadrupole deformation parameter γ. Therefore, γ has the optimal value for each given value of β. The definition of β and γ is given in Ref. [31]. Then, we project out the

eigenstate of the total angular momentum $\hat{J}$ from the optimized wave function, $\Phi^{J\pi}_{MK}(\beta) = \hat{P}^J_{MK}\Phi^\pi(\beta)$. $\Phi^{J\pi}_{MK}(\beta)$ is referred as AMD wave function in the following. Finally, we superpose all of the AMD wave functions on the energy surface that have the same parity and the angular momentum but have different K and β,

$$\Phi^{J\pi}_n = c_n\Phi^{J\pi}_{MK}(\{\beta\}) + c'_n\Phi^{J\pi}_{MK'}(\{\beta'\}) + \cdots .$$

The coefficients c_n, c'_n,... are determined by solving the Hill-Wheeler equation [34]. $\Phi^{J\pi}_n$ will be referred as AMD+GCM wave function.

We have investigated the single particle configuration of each intrinsic wave function by the AMD+HF method [31]. Once we obtain the intrinsic wave function, $\Phi_{\rm int}(\beta)$, we transform the single particle wave packet φ_i into the orthnormalized basis $\widetilde{\varphi}_\alpha$,

$$\widetilde{\varphi}_\alpha = \sum_{i=1}^{A}\frac{1}{\sqrt{\lambda_\alpha}}c_{i\alpha}\varphi_i,$$

where λ_α and $c_{i\alpha}$ are the eigenvalue and eigenvector of the matrix $B_{ij}=\langle\varphi_i|\varphi_j\rangle$. From this new basis function, we construct and diagonalize the Hartree-Fock single particle Hamiltonian,

$$\begin{aligned} h_{\alpha\beta} &\equiv \langle\widetilde{\varphi}_\alpha|\hat{t}|\widetilde{\varphi}_b\rangle + \sum_{\gamma=1}^{A}\langle\widetilde{\varphi}_\alpha\widetilde{\varphi}_\gamma|\hat{v}_n + \hat{v}_c|\widetilde{\varphi}_\beta\widetilde{\varphi}_\gamma - \widetilde{\varphi}_\gamma\widetilde{\varphi}_\beta\rangle, \\ &+ \frac{1}{2}\sum_{\gamma,\delta=1}^{A}\langle\widetilde{\varphi}_\gamma\widetilde{\varphi}_\delta|\widetilde{\varphi}^*_\alpha\widetilde{\varphi}_\beta\frac{\partial\hat{v}_n}{\partial\rho}|\widetilde{\varphi}_\gamma\widetilde{\varphi}_\delta - \widetilde{\varphi}_\delta\widetilde{\varphi}_\gamma\rangle, \\ h_{\alpha\beta}f_{\beta s} &= \epsilon_s f_{\alpha s}. \end{aligned}$$

The eigenvalue and eigenvector provide the single particle energy ϵ_s and the single particle wave function $\psi_s = \sum_{\alpha=1}^{A} f_{\alpha s}\widetilde{\varphi}_\alpha$. To investigate the properties of the single particle wave functions, we also calculate the magnetic quantum number $\langle\psi_s|\hat{j_z}|\psi_s\rangle$ and the amount of the positive-parity component $\langle\psi_s|\hat{P}^+|\psi_s\rangle$. We note that by this method we obtain only the occupied states. In the following, we denote the neutron m particle and n hole configuration relative to the N=20 spherical shell closure as $mpnh$.

Fig. 1 shows the calculated energy surface of the positive- and negative-parity states. There are three local minima in the positive-parity state and two local minima in the negative-parity state. Though we do not assume the axial symmetry, the wave functions on the energy surfaces are almost axially symmetric except for those located at the transitional region between the energy minima. These minima have different neutron single particle configurations. Fig. 2 shows the single particle orbitals occupied by the last 11 neutrons in the positive-parity state (a) and the negative-parity state (b). In this figure, the asymptotic quantum number $[N, n_z, l_z, j_z]$ of each orbital evaluated from its parity and magnetic quantum number is also shown. In the following, we

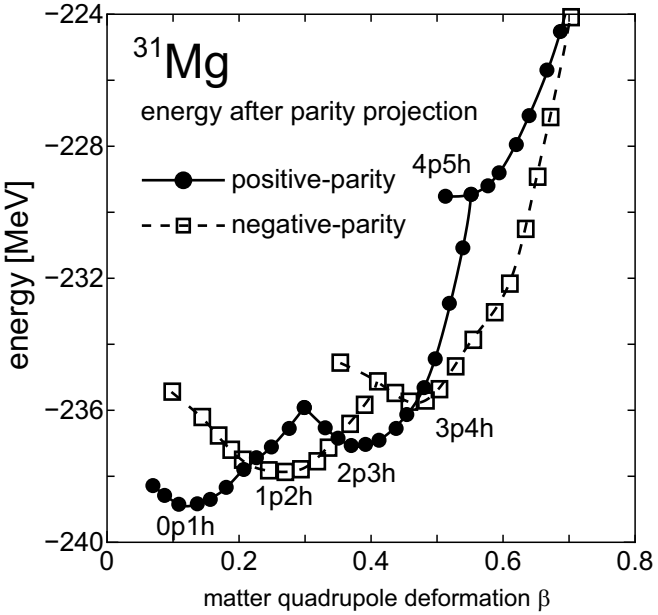

FIG. 1: Energy surfaces of ^{31}Mg as functions of matter quadrupole deformation parameter β for the positive- and negative-parity states. The estimated neutron particle hole configurations are also shown around the energy minima.

use the asymptotic quantum number to specify each neutron orbital. Fig. 2 (a) shows that in the spherical region of the positive-parity state, the last neutron particle or the neutron hole occupies [2,0,2,3/2] orbital that originates in the $0d_{3/2}$-orbital. Therefore this configuration is understood as the $0p1h$ configuration. Around $\beta \sim 0.3$, the neutron configuration changes from $0p1h$ to $2p3h$. The last two neutron occupy [3,3,0,1/2] orbital that intrudes from the pf-orbital. And a neutron hole occupies [2,0,0,1/2] orbital that originates in the $0d_{3/2}$-orbital. Around $\beta \sim 0.5$, the neutron configuration changes from $2p3h$ to $4p5h$. [2,0,2,3/2] and [2,0,0,1/2] orbitals are no longer occupied. Both of [3,3,0,1/2] and [3,2,1,3/2] orbitals intruding from the pf-orbital are occupied by two neutrons. A neutron hole is in [2,0,2,5/2] orbital that originates in the $0d_{5/2}$-orbital. In the same way, Fig. 2 (b) shows that there are two different neutron configurations $1p2h$ and $3p4h$ in the negative-parity state. The $1p2h$ configuration has the last neutron in [3,3,0,1/2] orbital and [2,0,2,3/2] orbital is unoccupied. Around $\beta \sim 0.4$ the configuration changes from $1p2h$ to $3p4h$. The $3p4h$ configuration has the last neutron in [3,2,1,3/2] orbital and both of [2,0,2,3/2] and [2,0,0,1/2] orbitals are unoccupied. Thus, the analysis of the single particle configurations has revealed that the minima of the positive-energy state correspond to the neutron $0p1h$, $2p3h$ and $4p5h$ configurations and those of the negative-parity state correspond to the neutron $1p2h$ and $3p4h$ configurations. It is also mentioned that protons are always below the Z=20 shell closure and do not excited from the $0p$-orbital to the $1s0d$-orbital, though the or-

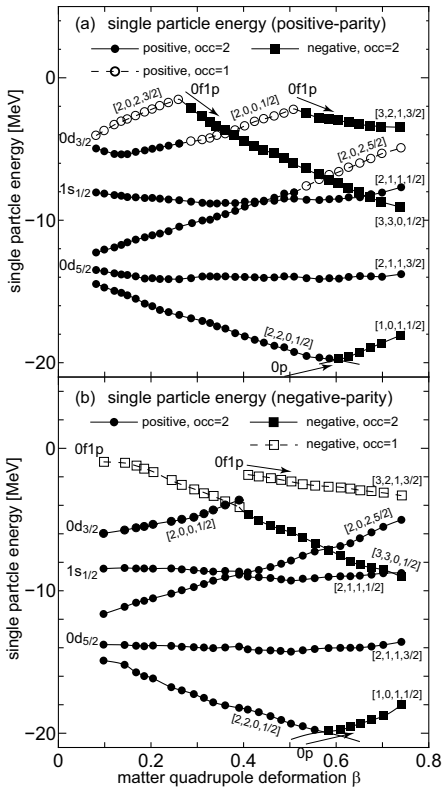

FIG. 2: The single particle orbitals of the last 11 neutrons of the positive-parity state (a) and the negative-parity state (b). Filled (open) symbols show the orbitals occupied by two (one) neutrons. Circles (boxes) show the orbital in which the amount of the positive-parity component is larger than (smaller than) 50%.

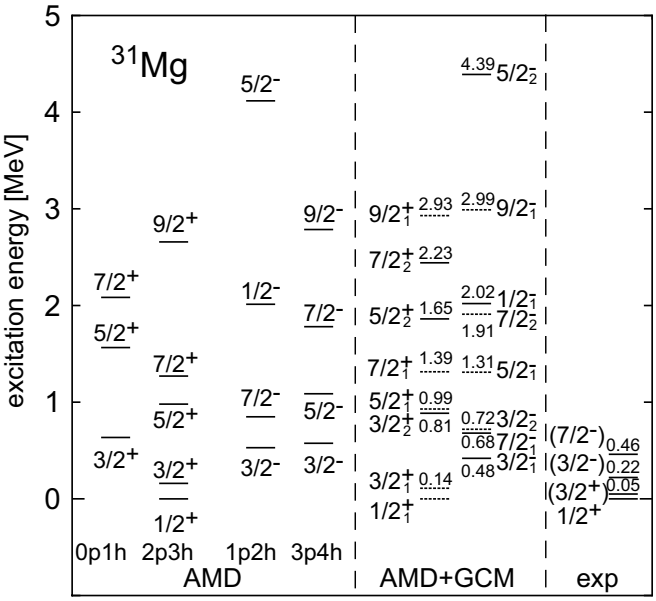

FIG. 3: Level scheme of ^{31}Mg obtained by the AMD wave functions at energy minima and by the AMD+GCM calculation together with the partial level scheme suggested in Ref. [16]. Solid (dashed) lines show the states dominated by the neutron $0p1h$ or $1p2h$ ($2p3h$ or $3p4h$) configurations. Numbers above or blow the states show the calculated and observed excitation energy in MeV.

der of the proton [2,2,0,1/2] and [1,0,1,1/2] orbitals has changed in the strongly deformed region. Therefore, the parity of total system depends only on the neutron configuration. There are some additional comments on Fig. 1 and 2. (1) All of the $mpnh$ configurations except for the $4p5h$ configuration appear at very small excitation energy. The energy difference between the lowest one ($0p1h$) and the highest one ($3p4h$) is less than 5 MeV. This leads to the coexistence of these particle-hole configurations within small excitation energy after the angular momentum projection as shown later. (2) The behavior of the neutron single particle orbitals of the positive- and negative-parity states are qualitatively similar to each other. As deformation becomes larger, [3,3,0,1/2] and [3,2,1,3/2] orbital originate in the pf-orbital come down and [2,0,2,3/2] and [2,0,0,1/2] orbital originate in the $0d_{3/2}$-orbital go up and cross to each other. The change of the particle hole configuration occurs just around the crossing points of these orbitals. This explains why the particle hole configurations appear in the order of the particle and hole numbers as deformation becomes larger. It is also mentioned that the behavior of the single particle orbital is qualitatively understood by the Nilsson model and it may explain why the Nilsson model calculation was qualitatively successful in Ref. [17]. (3) The energy of the $4p5h$ configuration is exceptionally higher than others and it is understood as follows. As explained above, the change of the neutron particle-hole configuration is caused by the crossing of four neutron orbitals that originate in the pf- and $0s1d$-orbitals. Therefore, up to four particle or four hole configuration can appear at small excitation energy, but more than five particle or hole configuration appear at rather high excitation energy. This feature is common to other neighboring nuclei such as Ne isotopes [26, 30] and Mg isotopes [27].

After the variational calculation, we have performed the angular momentum projection of the wave functions on the energy surfaces. The left side of FIG. 3 shows the excitation energies of the AMD wave functions at the energy minima. In the case of the positive-parity state, the $0p1h$ minimum generates the $3/2^+$, $5/2^+$ and $7/2^+$ states and the $2p3h$ minimum generates the $K^\pi=1/2^+$ rotational band with negative decoupling parameter. The $4p5h$ minimum generates the $K^\pi=5/2^+$ rotational band, but it is not shown since it is not involved in the low-lying states even after the GCM calculation. In the case of the negative-parity state, $1p2h$ minimum generates the $K^\pi=1/2^-$ rotational band with the large negative decoupling parameter $a \sim -4$ (the last neutron that occupy the $0f_{7/2}$ gives $a=-4$). It is interesting that the lowest

decay from ^{31}Na(g.s.)					decay to ^{31}Al			
^{31}Mg(J^π)	E_x (MeV)	log ft	$0p1h$ (%)	$2p3h$ (%)	^{31}Al(J^π)	E_x (MeV)	log ft	$2p4h$ (%)
$1/2^+_1$	0	4.6	0	93	$1/2^+_1$	1.22	6.1	5
$3/2^+_1$	0.14	5.2	25	61	$3/2^+_1$	1.81	5.8	10
$3/2^+_2$	0.81	5.8	68	20	$1/2^+_2$	3.08	5.2	69
$5/2^+_1$	0.89	5.3	21	63	$3/2^+_2$	3.83	5.0	61
$5/2^+_2$	1.85	5.9	67	11	$3/2^+_3$	4.11	4.8	79
					$1/2^+_3$	4.43	5.2	67

TABLE I: The calculated log ft values of the β-decay from the ground state of ^{31}Na to the low-lying states of ^{31}Mg and from the ground state of ^{31}Mg to the low-lying states of ^{31}Al.

state of $1p2h$ configuration is not $7/2^-$ but $3/2^-$ because of its deformation. The $3p4h$ configuration generates the K^π=$3/2^-$ rotational band. As clearly seen, the energy of the deformed states becomes lower. For example, the $3/2^-$ state that has the $3p4h$ configuration is lowered by about 5.1 MeV from the minimum of the energy surface, while the $3/2^+$ state that has the $0p1h$ configuration is lowered only by about 1.8 MeV. This leads to the coexistence of many particle-hole states within quite small excitation energy. However, it should be noted that there is no $1/2^+$ state except for the $2p3h$ configuration. It is also mentioned that the K quantum number of the deformed bands (K^π=$1/2^+$, $1/2^-$ and $3/2^-$) correspond to the asymptotic quantum number j_z of the last neutron particle or hole.

To complete our calculation, we have performed the GCM calculation by superposing all of the AMD wave functions on the energy surfaces. The calculated level scheme is shown in the middle of FIG. 3. There are mixing between different particle-hole configurations. For example, in the case of the $3/2^+$ states, the mixing between the $0p1h$ and $2p3h$ configurations lowers the energy of the $3/2^+_1$ state that has the dominant $2p3h$ configuration, while it pushes up the $3/2^+_2$ state that has the dominant $0p1h$ configuration. Since the AMD+GCM wave function is the sum of many Slater determinants, its particle-hole configuration is ambiguous. To evaluate it, we have calculated the squared overlap between the AMD+GCM wave function of each state and the AMD wave function at each energy minima that has the definite particle-hole configuration. The energy gain by such configuration mixing does not exist in the case of the $1/2^+_1$ state that purely consist of $2p3h$ configuration (it has no overlap with the $0p1h$ AMD wave function but has 93% overlap with the $2p3h$ AMD wave function), but it is the ground state with a small margin and consistent with the experiment [16]. The calculated total binding energy is 242.9 MeV. The excitation spectrum also shows the good agreement with the most recent spin-parity assignment [16]. The first excited state is the $3/2^+_1$ state that has the dominant $2p3h$ configuration. The squared overlap with the $2p3h$ AMD wave function amounts to 61%. The low-lying negative-parity states appear as the second ($3/2^-_1$), third ($7/2^-_1$) and fourth ($3/2^-_2$) excited states with the dominant $1p2h$, $1p2h$ and $3p4h$ configurations, respectively. The normal configuration ($0p1h$) appears as the fifth excited state $3/2^+_2$ at 0.81 MeV. Thus, from $0p1h$ to $3p4h$ states, many particle-hole configurations coexist below 1 MeV.

J^π	Q	Q_s	J^π	Q	Q_s
$3/2^+_1$	-18.9	-17.1	$3/2^+_2$	8.2	7.4
$5/2^+_1$	-19.1	-21.6	$5/2^+_2$	4.8	-2.7
$7/2^+_1$	-23.2	-22.5	$7/2^+_2$	-2.4	-5.3
$9/2^+_1$	-17.2	-19.5			

TABLE II: The electric quadrupole moment of the positive-parity states calculated by the AMD+GCM wave function (Q) and the rigid rotor approximation (Q_s).

Finally, we discuss observables and compare them with available experimental data. The magnetic moments of the ground state ($1/2^+_1$) and the first excited state ($3/2^+_1$) calculated without the spin quenching factor are $-0.91\mu_N$ and $0.43\mu_N$, respectively. The magnetic moment of the ground state shows the reasonable agreement with the observed value $-0.89\mu_N$ [16] and the shell model result[17], while $3/2^+_1$ state has the opposite sign to the ground state. The log ft value of the β decay from ^{31}Na and to ^{31}Al are summarized in TABLE I. The ground state of ^{31}Na and the low-lying states of ^{31}Al are also calculated by the AMD+GCM. The squared overlaps between the AMD+GCM wave function and the AMD wave function are also listed to show the particle-hole nature of the low-lying states ^{31}Mg and ^{31}Al. It is found that the ground state of ^{31}Na ($3/2^+$) is the mixture of the neutron $0p0h$, $2p2h$ and $4p4h$ configurations. The squared overlaps amount to 10%, 70% and 5%, respectively. These configurations feed the $0p1h$, $2p3h$ and $4p5h$ configurations of ^{31}Mg. Here, we must recall that the ground state of ^{31}Mg purely consist of the $2p3h$ configuration. Therefore, it is populated only from the $2p2h$ configuration of ^{31}Na that is the dominant component of the ^{31}Na. Indeed, the calculated log ft shows the stronger ^{31}Na(g.s.) $\rightarrow$ ^{31}Mg(g.s.) transition than others. It is also notable that the excited states of ^{31}Mg dominated by the $2p3h$ configuration have stronger transition than those dominated by the $1p2h$ configuration. Though the spin-parity assignment of the excited states are not fixed yet, the tendency of the log ft is comparable with the

experiment [4, 10]. The β-decay from ^{31}Al also reflects the specific charactor of the ^{31}Mg. Since, the ground state of ^{31}Mg purely consist of the neutron $2p3h$ configuration, it feeds only the neutron $2p4h$ configuration of ^{31}Al. The low-lying states of ^{31}Al are dominated by the neutron normal configuration ($0p2h$) and the intruder configuration ($2p4h$). The $1/2^+_2$, $3/2^+_2$, $3/2^+_3$, and $1/2^+_3$ states dominated by the neutron $2p4h$ configuration have smaller $\log ft$ than those dominated by other neutron configurations. The strength of $\log ft$ and the excitation energy shows good agreement with the experimental data [17]. The spin-parity assignment of those ^{31}Al states are not experimental fixed yet, but the present result and the shell model calculation [17, 25] shows the reasonable agreement. Table. II summarizes the quadrupole moments of the positive-parity states calculated by the AMD+GCM wave function and those evaluated by the rigid rotor approximation [35],

$$Q_s = \frac{3K^2 - J(J+1)}{(J+1)(2J+3)} Q_0,$$

where the intrinsic quadrupole moment Q_0 is calculated from the intrinsic wave function $\Phi^{\pi}_{\rm int}(\beta)$ that is the dominant component of each state. The K quantum number is taken as $1/2$ for the states dominated by the $1p2h$ configuration and $3/2$ for those dominated by the $3p4h$ configuration. Due to the strong deformation, the yrast states that have the intruder configuration show large collectivity. It is also notable that the rigid rotor approximation qualitatively reproduces these states, even though there are the configuration mixing in the AMD+GCM calculation.

To summarize, we have investigated the low-lying level structure of ^{31}Mg. The observed property of the ground state including the spin-parity is successfully reproduced. The coexistence of the spherical normal configuration and the strongly deformed intruder configuration at vary small excitation energy is predicted. The analysis of the single particle orbital has shown that the neutron $0p1h$, $1p2h$, $2p3h$ and $3p4h$ configurations appear on the energy surface. The angular momentum projection leads to the coexistence of these configurations and the GCM calculation has shown the mixing between them. Among the obtained states, only the ground state consists of the pure neutron $2p3h$ configuration and its spin-parity $1/2^+$ originates in a neutron hole in the Nilsson $[2, 0, 0, 1/2]$ orbital. This specific charactor is reflected to the β-decay strengths from the ground state of ^{31}Na and to the low-lying states of ^{31}Al.

The author acknowledges helpful discussions with Prof. Y. Kanada-En'yo. Most of the computational calculations are carried out by the SX-5 super computer at Research Center for Nuclear Physics, Osaka University (RCNP). This work is a part of the Research Project for Study of Unstable Nuclei from Nuclear Cluster Aspects.

[1] C. Thibault *et al.*, Phys. Rev. C **12**, 644 (1975).
[2] G. Huber *et al.*, Phys. Rev. C **18**, 2342 (1978).
[3] C. Détraz *et al.*, Phys. Rev. C **19**, 164 (1979).
[4] D. Guillemaud-Mueller *et al.*, Nucl. Phys. A **426**, 37 (1984).
[5] T. Motobayashi *et al.*, Phys. Lett. B **346**, 9 (1995).
[6] X. Campi, H. Flocard, A. K. Kerman and S. Koonin, Nucl. Phys. A **251** 193, (1975).
[7] A. Poves and J. Retamosa, Phys. Lett. B **184**, 311 (1986).
[8] E. K. Warburton, J. A. Becker and B. A. Brown, Phys. Rev. C **41**, 1147 (1990).
[9] N. Fukunishi, T. Otsuka and T. Sebe, Phys. Lett. B **296**, 279 (1992).
[10] G. Klotz *et al.*, Phys. Rev. C **47**, 2502 (1993).
[11] B. V. Pritychenko, *et al.*, Phys. Lett. B **461**, 322 (1999); Phys. Lett. B **467**, 309 (1999).
[12] M. Keim *et al.*, Eur. Phys. J. A **8**, 31 (2000).
[13] K.Yoneda, *et al.*, Phys. Lett. B **499**, 233 (2001).
[14] Nummela, *et al.*, Phys. Rev. C **64**, 054313 (2001).
[15] Y. Yanagisawa, *et al.*, Nucl. Phys. A **734**, 374 (2004).
[16] G. Neyens *et al.*, Phys. Rev. Lett. **94**, 022501 (2005).
[17] F. Marechal *et al.*, Phys. Rev. C **72**, 044314 (2005).
[18] B. H. Wildenthal, M. S. Curtin and B. A. Brown, Phys. Rev. C **28**, 28 (1983).
[19] A.Poves and J.Retamosa, Nucl. Phys. A **571**, 221 (1994).
[20] Y.Utsuno, T.Otsuka, T.Mizusaki and M.Honma, Phys. Rev. C **60**, 054315 (1999).
[21] Y. Utsuno, T. Otsuka, T. Glasmacher, T. Mizusaki and M. Honma, Phys. Rev. C **70**, 044307 (2004).
[22] D.J.Dean, *et al.*, Phys. Rev. C **59**, 2474 (1999).
[23] R. R. Rodriguez-Guzman, J. L. Egido and L. M. Robledo, Phys. Rev. C **62**, 054319 (2000).
[24] E. Caurier, F. Nowacki, A. Poves and J. Retamosa, Phys. Rev. C **58**, 2033 (1998).
[25] E. Caurier, F. Nowacki and A.Poves, Nucl. Phys. A **693**, 374 (2001).
[26] M. Kimura and H. Horiuchi, Prog. Theor. Phys. (Kyoto) **111**, 841 (2004).
[27] M. Kimura and H. Horiuchi, Prog. Theor. Phys. (Kyoto) **107**, 33 (2002).
[28] M. Yamagami and N. Van Giai, Phys. Rev. C **69**, 034301 (2004).
[29] Y. Kanada-En'yo, H. Horiuchi and A. Ono, Phys. Rev. C **52**, 628 (1995).
[30] Y.Kanada-Enyo, M. Kimura and H.Horiuchi, C. R. Physique **4**, 497 (2003).
[31] A. Dote and H. Horiuchi, Phys. Rev. C **56**, 1844 (1997).
[32] M. Kimura and H. Horiuchi, Phys.Rev. C **69**, 044319 (2004).
[33] J. Dechargé and D. Gogny, Phys. Rev. C **21**, 1568 (1980).
[34] D. L. Hill and J. A. Wheeler, Phys. Rev. **89**, 112 (1953).
[35] A. Bohr and B. R. Mottelson: Nuclear Structure, Vol. II (World Scientific, New York, 1975).